

---

# Dosimetry and Radiographic Analysis of $^{131}\text{I}$ -Labeled Anti-Tenascin 81C6 Murine Monoclonal Antibody in Newly Diagnosed Patients with Malignant Gliomas: A Phase II Study

Gamal Akabani, PhD<sup>1</sup>; David A. Reardon, MD<sup>2</sup>; R. Edward Coleman, MD<sup>1</sup>; Terence Z. Wong, MD<sup>1</sup>; Scott D. Metzler, PhD<sup>1</sup>; James E. Bowsher, PhD<sup>1</sup>; Daniel P. Barboriak, MD<sup>1</sup>; James M. Provenzale, MD<sup>1</sup>; Kim L. Greer<sup>1</sup>; David DeLong, PhD<sup>1</sup>; Henry S. Friedman, MD<sup>2</sup>; Allan H. Friedman, MD<sup>3</sup>; Xiao-Guang Zhao, MD<sup>1</sup>; Charles N. Pegram<sup>4</sup>; Roger E. McLendon, MD<sup>4</sup>; Darell D. Bigner, MD, PhD<sup>4</sup>; and Michael R. Zalutsky, PhD<sup>1</sup>

<sup>1</sup>Department of Radiology, Duke University Medical Center, Durham, North Carolina; <sup>2</sup>Department of Medicine, Duke University Medical Center, Durham, North Carolina; <sup>3</sup>Department of Surgery, Duke University Medical Center, Durham, North Carolina; and <sup>4</sup>Department of Pathology, Duke University Medical Center, Durham, North Carolina

---

The objective was to perform dosimetry and evaluate dose-response relationships in newly diagnosed patients with malignant brain tumors treated with direct injections of  $^{131}\text{I}$ -labeled anti-tenascin murine 81C6 monoclonal antibody (mAb) into surgically created resection cavities (SCRCs) followed by conventional external-beam radiotherapy and chemotherapy. **Methods:** Absorbed doses to the 2-cm-thick shell, measured from the margins of the resection cavity interface, were estimated for 33 patients with primary brain tumors. MRI/SPECT registrations were used to assess the distribution of the radiolabeled mAb in brain parenchyma. Results from biopsies obtained from 15 patients were classified as tumor, radionecrosis, or tumor and radionecrosis, and these were correlated with absorbed dose and dose rate. Also, MRI/PET registrations were used to assess radiographic progression among patients. **Results:** This therapeutic strategy yielded a median survival of 86 and 79 wk for all patients and glioblastoma multiforme (GBM) patients, respectively. The average SCRC residence time of  $^{131}\text{I}$ -mu81C6 mAb was 76 h (range, 34–169 h). The average absorbed dose to the 2-cm cavity margins was 48 Gy (range, 25–116 Gy) for all patients and 51 Gy (range, 27–116 Gy) for GBM patients. In MRI/SPECT registrations, we observed a preferential distribution of  $^{131}\text{I}$ -mu81C6 mAb through regions of vasogenic edema. An analysis of the relationship between the absorbed dose and dose rate and the first biopsy results yielded a most favorable absorbed dose of 44 Gy. A correlation between decreased survival and irreversible neurotoxicity was noted. A comparative analysis, in terms of median survival, was performed with previous brachytherapy clinical studies, which showed a proportional relationship between the average boost absorbed dose and the median survival. **Conclusion:** This study shows that

$^{131}\text{I}$ -mu81C6 mAb increases the median survival of GBM patients. An optimal absorbed dose of 44 Gy to the 2-cm cavity margins is suggested to reduce the incidence of neurologic toxicity. Further clinical studies are warranted to determine the effectiveness of  $^{131}\text{I}$ -mu81C6 mAb based on a target dose of 44 Gy rather than a fixed administered activity.

**Key Words:** radioimmunotherapy; tenascin-C; gliomas; brain tumors; dosimetry

**J Nucl Med 2005; 46:1042–1051**

---

**I**n spite of intensive clinical research, the improvement in survival for patients with malignant glioma has been minimal. The median survival for newly diagnosed and recurrent glioblastoma multiforme (GBM) patients remains dismal. More than 90% of all recurrences are adjacent to the site of origin, indicating that the failure of local tumor control represents a major factor (1–6). Adjuvant therapies using advanced radiation delivery methods are under investigation to increase local tumor control while minimizing damage to normal brain tissue. Radiosurgery and brachytherapy have been used to focally escalate the radiation dose for newly diagnosed GBM patients and as rescue therapy for patients with recurrent disease (7,8). A randomized clinical trial in newly diagnosed malignant gliomas performed by the Brain Tumor Cooperative Group established the efficacy of brachytherapy (9). The median survival for patients undergoing brachytherapy, radiation therapy, and chemotherapy was 64 versus 52 wk for those receiving only external-beam radiotherapy (XRT) and chemotherapy.

Our efforts have focused on administering a tumor-associated radiolabeled monoclonal antibody (mAb) directly

---

Received Dec. 3, 2004; revision accepted Jan. 24, 2005.  
For correspondence or reprints contact: Michael R. Zalutsky, PhD, Department of Radiology, Duke University Medical Center, Box 3808, Durham, NC 27710.  
E-mail: zalut001@mc.duke.edu

into a surgically created resection cavity (SCRC) to localize therapy of tumor foci within the tumor resection margins. We have used the mAb 81C6, a murine IgG<sub>2b</sub> protein that binds to an epitope within the alternatively spliced fibronectin type III region of tenascin-C (TN-C), which is an extracellular matrix (ECM) glycoprotein expressed ubiquitously in high-grade gliomas but not in normal brain (10,11). This mAb has previously undergone extensive preclinical and clinical evaluations (12–14).

We previously performed a phase I clinical trial to establish the maximum tolerated dose (MTD) of <sup>131</sup>I-labeled anti-tenascin murine 81C6 (<sup>131</sup>I-mu81C6) mAb injected into the intact SCRC of newly diagnosed patients (14). The established MTD was 4,440 MBq (120 mCi) of <sup>131</sup>I-mu81C6 mAb, and delayed neurologic toxicity was dose limiting. We present the dosimetric, radiographic, and corresponding dose–response relationships in this phase II clinical study in newly diagnosed and untreated adult patients with malignant gliomas. The clinical findings of this phase II study have been previously described in a separate study (15).

## METHODS AND MATERIALS

### Patient Characteristics

Thirty-three patients were treated in this phase II clinical trial: 23 men and 10 women with an average age of 49 y (range, 19–69 y). Twenty-seven patients had GBM, 4 had anaplastic astrocytoma (AA), and 2 had anaplastic oligodendroglioma (AO). All patients had a Karnofsky Performance Status (KPS) greater than 70, with a mean of 97. Patients were prescribed an administered dose of 4,440 MBq/20 mg of <sup>131</sup>I-mu81C6 mAb based on the MTD previously determined in a phase I clinical trial (14). However, 1 patient received a lower administered activity of 1,369 MBq (37 mCi). Twenty-nine patients received conformal fractionated or hyperfractionated XRT and 4 patients did not receive XRT. All but 5 patients were subsequently treated with adjuvant chemotherapy that consisted of one or more of the following agents: chloroethylcyclohexylnitrosourea, temozolomide (Temodar; Schering Co.), etoposide (VP-16), irinotecan (Camptosar; Pfizer Inc.), and tamoxifen. Patients were evaluated every month after adjuvant chemotherapy with a complete physical and neurologic examination, a KPS rating, and MRI with contrast-enhancing media administration. Patients were monitored for toxicity and response until progressive disease or death. As of November 2004, 3 patients remained alive (1 GBM, 1 AA, 1 AO) and continue to undergo periodic follow-up.

### Characteristics of <sup>131</sup>I-mu81C6 mAb

81C6 is an IgG<sub>2b</sub> mAb that binds to TN-C, a tumor-associated ECM oligomeric glycoprotein that is ubiquitously present in human gliomas but not present in normal brain. TN-C plays a significant role in a variety of cellular processes that facilitate astrocytic tumor cell invasion and migration, endothelial cell spreading, adhesion, and proliferation (10,16). Also, the distribution and intensity of TN-C correlates well with tumor neovascularity with more evident expression in aggressive histotypes and in those tumors with high proliferation indices (17–19). Therefore, the morphologic distribution of TN-C makes it an ideal target in radioimmunotherapy (RIT) for patients with malignant glioma.

The radionuclide <sup>131</sup>I has a physical half-life of 8.04 d, and it is a  $\beta$ -particle emitter with average and maximum energies of 181.7 and 806.9 keV, respectively. Its main  $\gamma$ -emission is 364.5 keV (81.2%). The 90th percentile distance ( $X_{90}$ ) for <sup>131</sup>I  $\beta$ -particles is 0.83 mm in liquid water, making it ideal for delivering highly localized absorbed doses to the interface of the SCRC and tumor foci.

The 81C6 mAb was grown in athymic mice in ascites form, purified over a Sepharose–staphylococcal protein A column followed by polyethyleneimine ion-exchange chromatography, and labeled using a modified IODO-GEN (Pierce Chemical Co.) procedure. The immunoreactivity of all preparations was >75%, with >95% eluting on size-exclusion high-performance liquid chromatography with a retention time corresponding to IgG.

### Administration of <sup>131</sup>I-mu81C6 mAb

Before RIT, MRI was obtained to document minimal residual disease of <1 cm and to corroborate the correct placement of the tip of the catheter within the SCRC. The radiolabeled mAb was injected into the SCRC via a Rickman reservoir where injections were performed in a fluoroscopy suite under sterile conditions. A needle was placed in the Rickman reservoir, and an equivalent amount of cerebrospinal fluid to the injection volume was withdrawn from the SCRC to reduce the possibility of cavity rupture. The administered volume varied between 3.0 and 5.0 mL among patients. However, for the case of small cavity sizes (<3 mL), when possible, a maximum amount of cerebrospinal fluid was withdrawn and a volume between 1 and 2 mL of the antibody was infused slowly for a period of 5–10 min.

### Toxicity Determinations

Patients were monitored for toxicity and response until death. Four to 6 wk after receiving <sup>131</sup>I-mu81C6 mAb therapy, patients received conformal fractionated or hyperfractionated XRT. Thereafter, patients with stable disease and with no grade 3 or greater hematologic toxicity received chemotherapy for up to 1 y. Patients were evaluated every month for a period of 1 y and every 3 mo thereafter. Serious toxicity was assessed using the National Cancer Institute Common Toxicity Criteria version 2.0 (20). Serious toxicity was defined as grade 3 or grade 4 nonhematologic toxicity or grade 4 hematologic toxicity lasting >28 d. Grade 3 or grade 4 neurologic toxicity consisted of coma, severe confusion, intractable seizures, severe weakness or paralysis, sensory loss, and severe coordination problems.

### Neuroimaging

MRI of the head was performed to assess radiographic changes in the cystic cavity and cavity margins. Gadolinium-enhanced T1-weighted axial MR images (3-mm-thick contiguous slices) were obtained after surgery, before therapy, immediately after therapy and discharge from isolation, and on a monthly basis thereafter for a minimum period of 1 y. MR images were used to assess radiographic changes, including volume measurements of the SCRC and enhancing rim. MRI obtained immediately after <sup>131</sup>I-labeled anti-tenascin 81C6 mAb administration was used as a baseline for future comparisons. In this manner, we were able to assess radiographic changes in SCRC volume and enhancing rim, albeit without definitive information about pathologic origin. Whenever possible, <sup>18</sup>F-FDG PET images were obtained and coregistered with MR images for comparison and correlation with histologic diagnoses after treatment.

## High-Energy SPECT

To assess the spatial distribution of  $^{131}\text{I}$ -mu81C6 mAb within the brain parenchyma, SPECT was performed using a high-energy rotating collimator as described elsewhere (21). SPECT images were reconstructed by ordered-subsets expectation maximization (22) with 2 iterations and 8 subsets. Detector spatial resolution and spatially varying collimator resolution, but not attenuation, were modeled within the image-reconstruction, forward-projection model. Scatter was estimated from a secondary energy window and incorporated into reconstruction by an additive model. High-energy SPECT studies were obtained before discharge from isolation and were coregistered with contrast-enhanced axial T1-weighted MR images of the head using fiducial markers. Coregistered images were used to assess the distribution of  $^{131}\text{I}$ -mu81C6 mAb in the SCRC and brain.

## Dosimetry

Absorbed dose estimates to the 2-cm cavity margins, bone marrow, and whole body (WB) were performed based on the methods previously described by Akabani et al. (13,14,23). Briefly, a 2-compartment system was used to describe the pharmacokinetics of  $^{131}\text{I}$ -mu81C6 mAb, where the first compartment is the SCRC and the second compartment is the WB. Serial WB scintigraphic images were used to assess the SCRC and WB clearance, where the clearance data from the SCRC and WB were fit to the functional solutions of a serial 2-compartment model and were expressed as:

$$A_{SCRC}(t) = A_0 e^{-(\lambda_p + \lambda_{SCRC})t}$$

$$A_{WB}(t) = A_0 \frac{\lambda_{SCRC}}{\lambda_{WB} - \lambda_{SCRC}} (e^{-\lambda_{SCRC}t} - e^{-\lambda_{WB}t}) e^{-\lambda_p t}, \quad \text{Eq. 1}$$

where  $A_0$  is the initial administered activity,  $\lambda_p$  is the physical decay constant of  $^{131}\text{I}$ , and  $\lambda_{SCRC}$  and  $\lambda_{WB}$  are the biologic clearance constants for the SCRC and WB, respectively. The residence time for the SCRC ( $\tau_{SCRC}$ ) and WB ( $\tau_{WB}$ ) were estimated from these clearance curves. The WB absorbed dose was estimated as:

$$D_{WB} = A_0(\tau_{WB}S(WB \leftarrow WB) + \tau_{SCRC}S(WB \leftarrow SCRC)), \quad \text{Eq. 2}$$

where  $S(WB \leftarrow WB)$  and  $S(WB \leftarrow SCRC)$  are the corresponding S values that are dependent on effective body weight. Absorbed dose estimates for bone marrow were based on time-activity measurements of  $^{131}\text{I}$  in blood acquired immediately after administration, where a reduction factor of 0.3 was used to assess the dose contribution from blood to bone marrow (13). Dose contributions from sources located in the SCRC and WB were also added. Thus, the absorbed dose to bone marrow was estimated as:

$$D_{BM} = 0.3D_{Blood} + A_0(\tau_{WB}S(BM \leftarrow WB) + \tau_{SCRC}S(BM \leftarrow SCRC)), \quad \text{Eq. 3}$$

where the S values to bone marrow from sources located in the SCRC,  $S(BM \leftarrow SCRC)$ , and WB  $S(BM \leftarrow WB)$  were  $8.6 \times 10^{-5}$  and  $1.3 \times 10^{-4}$  cGy MBq $^{-1}$  h $^{-1}$ , respectively. Absorbed doses to other organs and tissues have been addressed in a previous study (13).

To understand the effects of  $^{131}\text{I}$ -mu81C6 mAb on normal brain toxicity and tumor control, and resultant changes in MR images, it is important to determine the absorbed doses as a function of depth from the SCRC interface. T1-weighted contrast-enhanced axial MR images of the patient's head were obtained before therapy and

immediately after discharge from isolation to assess any potential acute radiographic changes. MR images were used to generate a 3-dimensional reconstruction of the head, and the volume of the SCRC was calculated using image analysis software. This volume was used to estimate the initial activity concentration in the SCRC at the time of administration.

We performed the dosimetry of the cavity margins using quantitative SPECT and the 3-dimensional discrete Fast Fourier Transform (FFT, \*) convolution method for  $^{131}\text{I}$  as described in detail elsewhere (23). Briefly, the dose rate to any given region within the brain is given by:

$$\dot{D}_{Brain} = \dot{a}(r,t) * K(r), \quad \text{Eq. 4}$$

where  $\dot{a}(r,t)$  represents the activity distribution within the brain, including the SCRC, as measured by SPECT, and  $K(r)$  represents the dose convolution kernel for the radionuclide  $^{131}\text{I}$ , which was estimated by means of Monte Carlo methods (23). The total absorbed dose is then estimated as:

$$D_{Brain}(r) = \int_0^{\infty} \dot{D}_{Brain}(r) dt = \int_0^{\infty} \dot{a}(r,t) * K(r) dt; \quad \text{Eq. 5}$$

however, assuming no significant changes in activity distribution, the absorbed dose can be expressed as  $D_{Brain}^{RIT} = \tilde{a}(r) * K(r)$ , where  $\tilde{a}(r)$  is the cumulated activity concentration within the brain, including the SCRC. A 2-cm region of interest around the SCRC was then drawn to assess the average absorbed dose to the cavity margins  $D_{CM}$ , given as:

$$D_{CM} = \frac{\int D_{Brain}(r) dv}{\int dv}, \quad \text{Eq. 6}$$

and the total absorbed is given as  $D_{CM}^{Total} = D_{CM} + D_{CM}^{XRT}$ , where  $D_{CM}^{XRT}$  is the dose delivered during XRT.

## RESULTS

### Distribution of mAb in SCRC and Brain Parenchyma

To assess the spatial distribution of  $^{131}\text{I}$ -mu81C6 within the brain parenchyma, high-energy SPECT was performed using a high-energy rotating collimator. SPECT images were registered with axial T1-weighted contrast-enhanced MR images that showed the effect of peritumoral vasogenic brain edema before therapy in the distribution of the radio-labeled mAb beyond the cavity interface. We analyzed the distribution of  $^{131}\text{I}$ -mu81C6 mAb in 18 patients, of whom 9 (8 GBM, 1 AO) showed an activity distribution beyond the cavity interface following the patterns of vasogenic edema. In some patients, this distribution extended beyond the 2-cm cavity margins. On the other hand, we observed that, in 9 patients without vasogenic edema, the activity distribution was well confined within the cavity. Distribution of  $^{131}\text{I}$ -mu81C6 mAb beyond the cavity interface was observed in all patients with brain vasogenic edema independent of cavity size. The ratio of average activity concentration in the 2-cm cavity margins and activity concentration in the SCRC was 0.26 (range, 0.11–0.38) and 0.05 (0.03–0.08) for pa-

tients with and without vasogenic edema, respectively. A *t* test with unequal variances showed this difference to be statistically significant ( $P < 0.05$ ). Therefore, at the macroscopic level, patients with vasogenic edema had approximately 5 times higher activity concentrations within the 2-cm cavity margins than those without vasogenic edema. As an example, Figure 1 shows a comparison of the activity distribution in selected patients with and without brain vasogenic edema. These *in vivo* results are consistent with previous *in vitro* studies, which have shown that when the blood–brain barrier (BBB) is disrupted, compounds distribute into regions of edema (24,25).

#### Overall Survival and Dosimetric Correlations

The average SCRC volume among all patients was 10.7 cm<sup>3</sup> (0.5–30.5 cm<sup>3</sup>), whereas 7 patients had SCRC volumes below 5.0 cm<sup>3</sup>. The average SCRC residence time of <sup>131</sup>I-mu81C6 mAb for all 33 patients was 76 h (range, 34–169 h). The average absorbed dose to the 2-cm cavity interface from <sup>131</sup>I-mu81C6 mAb among all patients and GBM patients who received XRT was 48 Gy (range, 25–116 Gy) and 51 Gy (27–116 Gy), respectively. The initial average dose rate to the 2-cm cavity interface among all patients was 0.68 Gy h<sup>-1</sup> (range, 0.26–1.8 Gy h<sup>-1</sup>). However, 2 patients received absorbed doses to the 2-cm cavity margins in excess of 110 Gy because of their small cavity size. Excluding these 2 patients, the average absorbed dose from <sup>131</sup>I-mu81C6 mAb among the 24 GBM patients was 45 Gy (range, 27–77 Gy) and the average initial dose rate was 0.63 Gy/h (range, 0.26–1.13 Gy/h). Table 1 provides a summary of the dosimetric results for patients with tumors of all pathologies and corresponding survival and related toxicity. The median survival among all patients and GBM patients was 87 wk (95% CI, 61–122 wk) and 79 wk (95% CI, 55–116 wk). Four GBM patients did not receive XRT. Excluding these 4 GBM patients, the average absorbed dose to the 2-cm-thick cavity interface from <sup>131</sup>I-mu81C6 mAb

was 44 Gy (range, 27–77 Gy) and the median survival for these 24 patients was 79 wk.

#### Hematologic Toxicity and WB and Bone Marrow Dosimetric Correlations

Grade IV hematologic toxicity developed in 13 patients, and the average WB and bone marrow dose for these patients was 71 cGy (range, 40–94 cGy) and 94 cGy (range, 67–111 cGy), respectively. On the other hand, the average WB and bone marrow dose for the patients without grade IV hematologic toxicity was 53 cGy (range, 14–96 cGy) and 78 cGy (range, 33–100 cGy), respectively. A Student *t* test with unequal variances showed a statistical significance between the 2 groups based on the WB dose ( $P < 0.01$ ). However, there was no correlation between bone marrow dose and hematologic toxicity ( $P > 0.05$ ).

#### Neurotoxicity and Dosimetric Correlations

Thirteen patients (12 GBM, 1 AO) had grade 3 or grade 4 irreversible neurologic toxicity (Table 1). The average absorbed dose and initial average dose rate to the 2-cm-thick margins from <sup>131</sup>I-mu81C6 mAb were 56 Gy (range, 32–116 Gy) and 0.77 Gy/h (0.4–1.8 Gy/h), respectively. However, 3 of these 13 patients (patients 9, 28, and 29) had small cavity volumes ( $\leq 5$  cm<sup>3</sup>), and extensive vasogenic edema with radiographic changes developed immediately after <sup>131</sup>I-mu81C6 mAb administration; these patients did not receive XRT. Therefore, these 3 patients were not considered in the following analysis. Among all patients who received <sup>131</sup>I-mu81C6 mAb and XRT, the total average absorbed dose to the 2-cm cavity margins was 107 Gy (range, 92–136 Gy).

The median survival for GBM patients in this group ( $n = 10$ ) was 73 wk (95% CI, 47–116 wk). In contrast, there were 19 patients (14 GBM, 4 AA, 1 AO) who had grade 1 through grade 4 reversible neurologic toxicity. These patients received an average absorbed dose and average initial

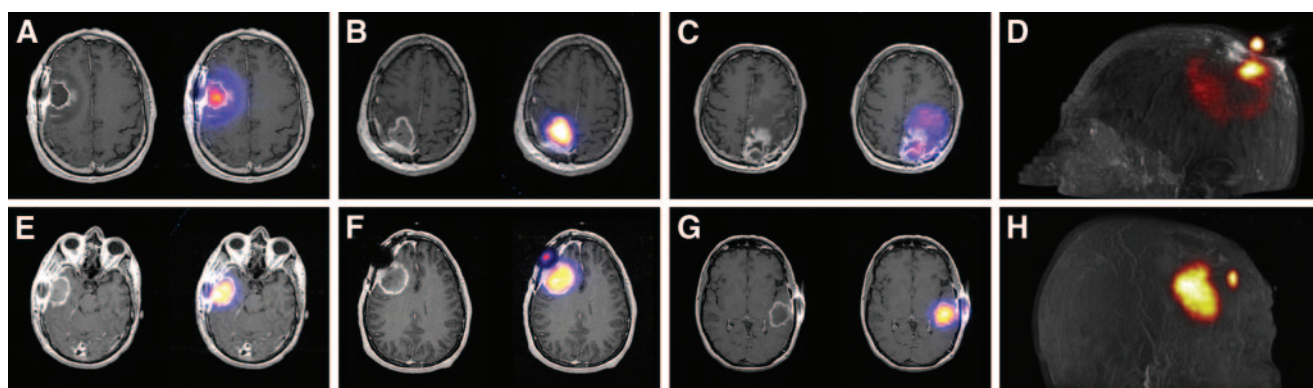


**FIGURE 1.** Effect of vasogenic edema in distribution of <sup>131</sup>I-mu81C6 mAb in brain parenchyma. MRI (left) and coregistered MRI/SPECT (right) images of patients with vasogenic edema (A–C) and without vasogenic edema (E–G). Average activity ratio between 2-cm cavity margins and SCRC was 0.26 (0.11–0.38) for patients with vasogenic edema, whereas the ratio for patients without vasogenic edema was 0.05 (0.03–0.08). Thus, activity concentrations within regions of vasogenic edema were a factor of 5 higher than in those regions without vasogenic edema. D and H represent a 3-dimensional maximum-intensity-projection view of activity distribution for patients described in C and F, respectively.

TABLE 1

Absorbed Dose Estimates, Survival, Neurologic and Hematologic Toxicity, and Biopsy Results for 33 Patients with Newly Diagnosed Gliomas Treated with <sup>131</sup>I-mu81C6 mAb

Patient no.	Dx	Sex and race	Age (y)	Weight (kg)	KPS	SCRC volume (cm <sup>3</sup> )	Adm. activity (MBq)	VE	$D_{CM}^{Max}$ (Gy/h)	$D_{CM}$ (Gy)	$D_{CM}^{XRT}$ (Gy)	$D_{CM}^{Total}$ (Gy)	$D_{WB}$ (cGy)	$D_{BM}$ (cGy)	Survival (wk)	Toxicity		
																NT	HT	Biopsy
1	GBM	MW	44	92	100	12.5	—	4,440	0.56	45	63	108	46	84	79	S (3)	3	
2	GBM	MW	47	83	100	8.6	—	4,440	0.66	52	63	115	46	81	87	S (2)	3	
3	GBM	MW	38	81	80	13.8	—	4,440	0.54	43	60	103	77	99	41		4	
4	GBM	FW	56	68	100	23.3	—	4,440	0.43	34	59	93	63	85	61	D (4, irr)	3	
5	GBM	MW	43	77	90	26.4	—	4,440	0.41	32	59	92	76	96	116	D (3, irr)	4	T
6	GBM	FB	48	79	70	8.5	—	4,440	0.66	52	59	111	81	100	304		4	R, R, T
7	GBM	FW	39	66	100	7.2	—	4,440	0.70	55	58	113	65	85	148	D (3, irr)	3	R
8	AA	MW	39	81	100	13.8	—	4,400	0.52	29	60	89	62	83	291*		3	
9	GBM	FW	58	72	80	2.1	—	4,440	1.13	73	—	73	43	72	39		3	
10	GBM	FW	35	61	100	8.7	—	4,440	0.65	50	59	110	79	89	268*	D (4)	4	R
11	AA	MW	19	88	100	12.9	—	4,440	0.56	38	64	102	48	81	89		3	T
12	GBM	MW	36	98	100	5.5	—	4,440	0.77	40	59	99	68	94	113		4	
13	GBM	MW	53	88	100	20.5	—	4,440	0.45	58	60	118	53	99	95	D (1)	4	T
14	GBM	MW	51	77	100	2.9	—	4,440	1.01	45	61	106	77	88	123		4	R, R, T
15	GBM	MW	55	84	100	3.8	—	4,440	0.90	35	75	110	40	68	172	D (3, irr)	4	R
16	GBM	MW	60	75	100	2.2	—	4,440	1.12	46	65	111	37	64	35	D (3)	3	
17	GBM	MW	50	97	100	17.9	+	4,440	0.48	42	60	102	25	73	55	D (3, irr)	3	T
18	AA	MW	38	69	100	9.4	—	4,440	0.63	25	61	86	69	78	219	D (2)	3	
19	GBM	MW	49	76	100	10.9	—	4,440	0.60	45	59	105	55	83	52	D (3, irr)	3	T + R
20	AO	MW	68	81	100	5.5	+	4,440	0.77	50	64	114	56	83	95	D (4, irr)	3	
21	AA	MW	46	81	100	5.2	—	4,440	0.79	27	63	90	74	85	58	D (3)	4	T
22	GBM	FW	47	71	100	8.0	—	4,440	0.67	42	60	102	56	78	77	D (4, irr)	3	R, T
23	GBM	FW	59	71	100	10.0	—	4,440	0.62	45	60	105	94	101	65	D (4, irr)	4	R
24	GBM	MW	60	72	100	8.1	+	4,440	0.67	34	60	94	48	71	73	D (3, irr)	3	R
25	GBM	MW	38	83	100	16.3	—	4,440	0.50	34	60	94	84	101	144		3	
26	GBM	MW	55	105	100	16.3	+	4,440	0.50	39	60	99	51	91	126		3	
27	AO	FW	35	54	100	12.2	—	4,440	0.57	51	—	51	96	96	230*	D (2)	3	
28	GBM	MW	63	70	80	1.2	+	4,440	1.35	116	—	116	44	78	24	A, S, D (3, irr)	3	
29	GBM	MW	53	90	100	0.5	+	4,440	1.80	113	—	113	74	97	97	A, S, D (3, irr)	4	T
30	GBM	FW	65	70	100	12.1	—	4,440	0.57	77	60	137	67	102	47	D (4, irr)	4	
31	GBM	MW	54	108	100	4.3	+	1,369	0.26	42	60	102	14	34	50		3	
32	GBM	MW	52	72	100	30.5	+	4,440	0.38	65	60	125	67	112	109		4	
33	GBM	FW	54	76	100	13.0	+	4,440	0.56	27	60	87	52	75	27		3	

\*Censored (alive).

Dx = diagnosis; VE = vasogenic edema; Adm. activity = administered activity;  $D_{CM}^{Max}$  = maximum initial dose rate;  $D_{CM}$  = dose from RIT;  $D_{CM}^{XRT}$  = dose from XRT;  $D_{CM}^{Total}$  = total dose from RIT and XRT;  $D_{WB}$  = WB dose;  $D_{BM}$  = bone marrow dose; NT = neurotoxicity; HT = hematologic toxicity (grade: 1, 2, 3, or 4); S = subacute; D = delayed (grade: 1, 2, 3, or 4; irr = irreversible); T = tumor; R = radionecrosis; A = acute.

dose rate to the 2-cm-thick cavity margins of 44 Gy (range, 25–73 Gy) and 0.64 Gy/h (range, 0.26–1.13 Gy/h), respectively, and a total absorbed dose, including XRT, of 97 Gy (range, 51–125 Gy). The median survival for this GBM group with reversible neurotoxicity was 98 wk (range, 39–126 wk) (95% CI, 39–126 wk), respectively. The results from this analysis are in accordance with our previous findings from our phase I clinical trial in which we found that absorbed doses and initial dose rates to the 2-cm cavity margins higher than 50 Gy and 0.6 Gy h<sup>-1</sup>, respectively, resulted in a higher probability of radiation injury (14). Figure 2A shows the Kaplan–Meier survival plots for

all patients and GBM patients and Figure 2B shows the Kaplan–Meier survival plots for GBM patients with reversible and irreversible neurologic toxicity. The median age among GBM patients with reversible and irreversible neurotoxicity was 51 y (range, 35–60 y) and 53 y (range, 39–65 y), respectively; thus, there was no correlation between irreversible neurotoxicity and age. Moreover, the preferential distribution of the radiolabeled mAb through regions of vasogenic edema led to immediate radiographic changes in only 4 of 9 patients; however, symptomatic changes were observed only in patients 28 and 29 due to small cavity sizes that generated dose rates higher than 1 Gy

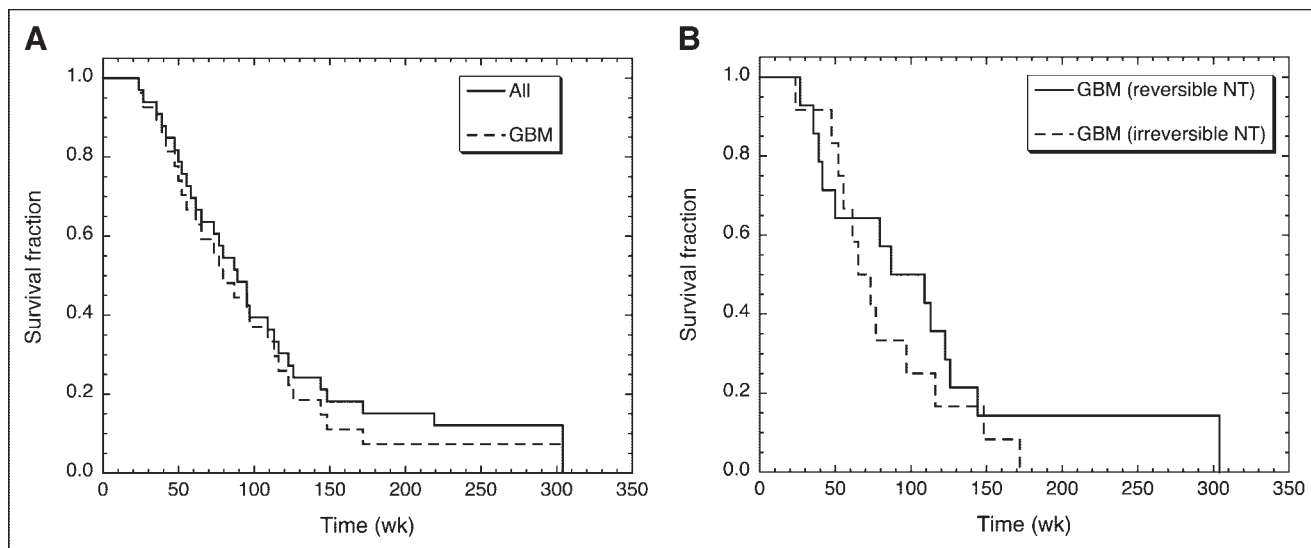


**FIGURE 2.** (A) Kaplan–Meier survival plot for all patients ( $n = 33$ ) and for GBM patients ( $n = 27$ ). Median survival for all patients and GBM patients was 89 wk (95% CI, 61–113 wk) and 79 wk (95% CI, 52–113 wk), respectively. (B) Kaplan–Meier survival plot for GBM patients with reversible or irreversible neurotoxicity. Median survival for GBM patients who received XRT with reversible ( $n = 14$ ) and irreversible neurotoxicity ( $n = 10$ ) was 98 wk (95% CI, 39–126 wk) and 73 wk (95% CI, 47–116 wk), respectively.

$h^{-1}$ . There was no significant statistical correlation between expression of vasogenic edema at the time of therapy and neurologic toxicity. Also, there was no statistical significant difference in the median survival among GBM patients with and without vasogenic edema.

### Neuroimaging Observations

MRI and  $^{18}\text{F}$ -FDG PET studies were used to follow the effects of  $^{131}\text{I}$ -mu81C6 mAb therapy and for achieving a better understanding of delayed tissue radiation necrosis (26). We evaluated the changes induced by  $^{131}\text{I}$ -mu81C6 mAb using MRI with coregistered PET (MRI/PET) on 32 patients. In these patients, an enhancing rim was observed on T1-weighted contrast-enhanced MR images within 4 wk after therapy that corresponded to coagulative necrosis. Vasogenic edema surrounding the SCRC was the most significant effect after  $^{131}\text{I}$ -mu81C6 mAb therapy and it resolved or was reduced to a minimum level within 2 mo after therapy. However, in some patients with irreversible neurotoxicity, vasogenic edema expanded once again and continued, and corticosteroids were necessary to alleviate neurologic symptoms.

Histopathologic correlation with initial biopsy samples showed that neovascularization, hyalinization of vascular walls, and gliosis were found in the periphery of the area where infiltration of macrophages to the necrotic area was well observed; moreover, further examination showed that sites at which the vascular walls were found to have acute-stage fibrinoid necrosis also showed coagulative necrosis. This uniform enhancing rim on T1-weighted MR images presented  $^{18}\text{F}$ -FDG activity levels between those generally observed in white and gray matter and it was not necessarily associated with tumor progression.

We reviewed sequential registered MRI/PET studies from 10 patients that were correlated with the biopsy diagnosis after treatment. The rim of  $^{18}\text{F}$ -FDG accumulation was seen on the first posttreatment scan obtained 1–3 mo after therapy and persisted unchanged over the 2- to 26-mo follow-up period. Pathologically, the nonmalignant rim was associated with a marked increase of macrophage infiltrates. However, in those patients with biopsy-proven tumor progression, nodularity of the rim was indicative of tumor progression (Fig. 3). These observations demonstrate that a rim of  $^{18}\text{F}$ -FDG accumulation observed after administration of  $^{131}\text{I}$ -mu81C6 mAb therapy is independent of the presence of malignant disease. However, malignant progression or recurrence is strongly suggested by the development of new intense hypermetabolic nodularity within the rim of  $^{18}\text{F}$ -FDG accumulation (27).

### Histopathology and Dosimetric Correlations

Twenty stereotactic biopsy samples were obtained from 15 patients. These biopsy samples were obtained from regions of new enhancement and high hypermetabolic activity as suggestive of tumor progression using registered PET/MR images at the first sign of symptomatic progression. Multiple biopsy samples were obtained at different time points from 3 patients (Table 1). We classified the results of these biopsies as tumor (T), tumor and radionecrosis (T + R), and radionecrosis (R). The first biopsies among all 15 patients were as follows: 6 biopsies were found to be tumor, 8 biopsies were found to be radionecrosis, and 1 was found to be a combination of tumor and radionecrosis. The average absorbed dose and average initial dose rate to the 2-cm cavity margins from  $^{131}\text{I}$ -mu81C6 mAb for those patients with radionecrosis was 47 Gy

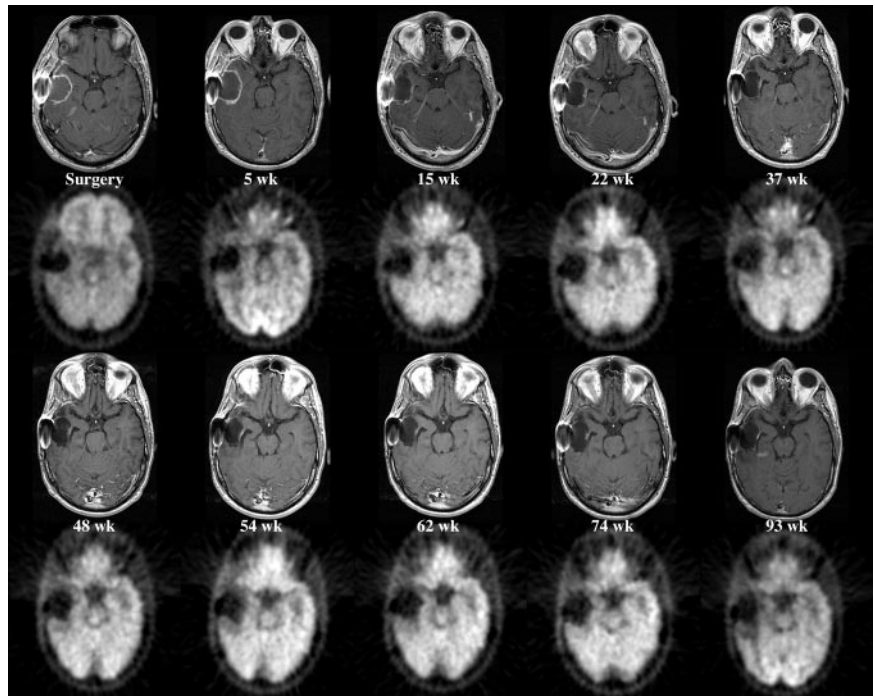


**FIGURE 3.** Sequential registered MRI/PET images from patient 15, who received 35 Gy to 2-cm cavity margins with an initial dose rate of 0.9 Gy h<sup>-1</sup>. A uniform rim in MRI was observed 1 mo after therapy and persisted unchanged over 59 wk with minimal vasogenic edema and minimal <sup>18</sup>F-FDG accumulation. Subsequently, grade III irreversible neurologic toxicity developed and, 118 wk after therapy, a biopsy sample was obtained, which indicated radionecrosis. However, 177 wk after therapy, new intense <sup>18</sup>F-FDG hypermetabolic nodularities and MRI enhancements with extensive vasogenic edema were observed on registered MRI/PET images, indicative of tumor progression.

(range, 34–55 Gy) and 0.66 Gy/h (0.62–0.70 Gy/h), respectively. For those patients with tumor only, the average absorbed dose and average initial dose rate was 39 Gy (range, 26–58 Gy) and 0.54 Gy/h (range, 0.41–0.71 Gy/h), respectively. However, patient 29 was not considered in this analysis because tumor recurrence was >2 cm away from the margins of the SCRC and was considered to be multifocal. The initial biopsy of patient 22 showed radionecrosis; however, a second biopsy after 45 wk established recurrent tumor and disease progression. Similarly, the first and second biopsies of patients 6 and 14 revealed radionecrosis, whereas a third biopsy obtained after 43 and 17 wk, respectively, showed tumor progression. Five patients with biopsy-proven radionecrosis and grade III or grade IV delayed irreversible neurologic toxicity received an average absorbed dose and dose rate of 42 Gy/h (range, 34–55 Gy/h) and 0.71 Gy/h (0.62–0.90 Gy/h), respectively. Three patients with biopsy-proven tumor and tumor plus radionecrosis had grade III irreversible neurologic toxicity.

Figure 4 presents a scatter plot of the first biopsy results showing the relationship between biopsy outcome on initial dose rate and average absorbed dose to the 2-cm cavity margins (average boost absorbed dose) delivered by <sup>131</sup>I-mu81C6 mAb. An optimal absorbed dose is defined as that dose which maximizes tumor control while minimizing the induction of radiation necrosis. We observed that the minimal absorbed dose for tumor control was approximately 42 Gy, whereas the median absorbed dose among patients with radionecrosis was 44.8 Gy, which is within the initial estimate of 44 Gy established previously in our phase I clinical trial (14). Moreover, this estimate is in agreement with the average absorbed dose of 44 Gy for patients in whom reversible neurologic toxicity developed.

#### Patterns of Failure and Reoperation

Of the 27 GBM patients, 1 patient was found to be free of tumor recurrence. Of the remaining 26 patients, local tumor progression developed in 23 patients, as defined by the development of new nodularities within 2-cm margins on MRI, hyperintense <sup>18</sup>F-FDG accumulation, and biopsy corroboration when possible. Distant multifocal disease developed in 2 patients. Only 1 patient underwent another operation for mass effect. As a whole, local recurrence comprised the major cause of failure in GBM patients

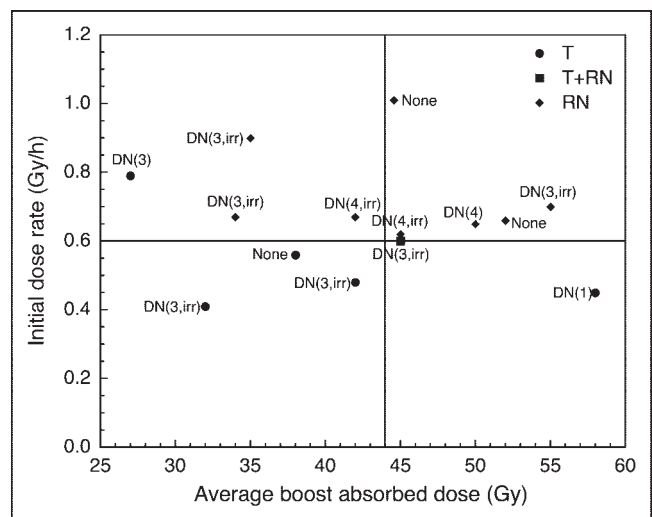


**FIGURE 4.** Scatter plot of biopsy results and neurologic toxicity among GBM tumor patients as function of average absorbed dose  $D_{CM}$  and maximum dose rate  $\dot{D}_{CM}^{max}$  to 2-cm cavity margins. T = tumor; RN = radionecrosis; DN = delayed neurotoxicity and grade 1, 2, 3, or 4; irr = irreversible.

(23/27, 85%), which is similar to that observed in brachytherapy.

## DISCUSSION

Understanding the therapeutic efficacy and deleterious effects of  $^{131}\text{I}$ -mu81C6 mAb therapy on normal brain tissue is of significance in the design of future treatment protocols with this promising agent. However, the sequence of events leading to the development of radiation injury and the minimum absorbed doses and dose rates required to induce these detrimental changes while maximizing tumor control are poorly understood. Our observations demonstrate that, similar to brachytherapy, the absorbed dose and dose rate appear to play a significant role in the development of normal brain injury, which can lead to either reversible or irreversible neurotoxicity.

Experimental and clinical data have demonstrated that, in general, the biologic effects of radiation injury in brain tissue diminish with decreased dose rate (28). Therefore, the same radiobiologic processes that are important for the biologic effects seen after fractionated XRT, radiosurgery, and brachytherapy should also be important for  $^{131}\text{I}$ -mu81C6 mAb therapy. Such processes include, but are not limited to, intrinsic cellular radiosensitivity, early sensitivity versus late-reacting normal tissue, repair of sublethal and potentially lethal damage, tumor invasiveness and cell population kinetics, cell cycle progression and redistribution, and reoxygenation (29).

Similar to brachytherapy, high-absorbed doses delivered at very low dose rates ( $<0.4$  Gy/h) produce very restricted areas of necrosis with surrounding edema that resolve with time; however, early tumor progression was the resulting endpoint (28). Conversely, doses higher than 50 Gy delivered at high dose rates ( $>0.6$  Gy/h) result in profound, irreversible changes, the extent of which depends on the dose and volume

of brain tissue irradiated (28). Mild symptomatic radiation necrosis may be treated with corticosteroid therapy; however, more severe and irreversible radionecrosis frequently requires reoperation to relieve symptoms and decrease the need for corticosteroids. Because the brain is so inefficient in removing necrotic tissue, clinical detrimental symptoms are regularly progressive if reoperation is delayed, where the mass of necrotic tissue and the rim of damaged normal brain tissue lead to factors that alter BBB function, which incites brain vasogenic edema. Reoperation and removal of necrotic tissue may result in a better quality of life and improvement in survival.

Similar to our previous phase I clinical study (14), the initial dose rate appears to play a major role in the development of radiographic enhancement and the corresponding symptomatic radionecrosis after therapy with  $^{131}\text{I}$ -mu81C6 mAb. In this phase II study we observed again that absorbed doses higher than 50 Gy and dose rates higher than  $0.6$  Gy  $\text{h}^{-1}$  resulted in radionecrosis in first-time biopsies, which is within the range of  $0.3$ – $0.6$  Gy/h established by Leibel et al. for high-dose-rate brachytherapy (28). Furthermore, clinical studies using radiosurgery and high-dose-rate brachytherapy have shown a proportional relationship between the boost absorbed dose and the median survival for treatment of newly diagnosed GBM patients. Figure 5 presents a plot of median survival as a function of the average boost absorbed dose for different clinical studies, including our phase I and phase II clinical trials (1,3–7,9,30–34). We observed an asymptotic median survival of approximately 86 wk for boost doses higher than 50 Gy among brachytherapy studies and 92 wk for RIT for absorbed doses higher than 80 Gy (35). This limiting effect in median survival can be explained as brachytherapy irradiates equally both normal tissue and tumor tissue with a very steep dose gradient; thus, normal brain tissue damage represents the major limiting factor in this adjuvant therapy strategy, leading to high

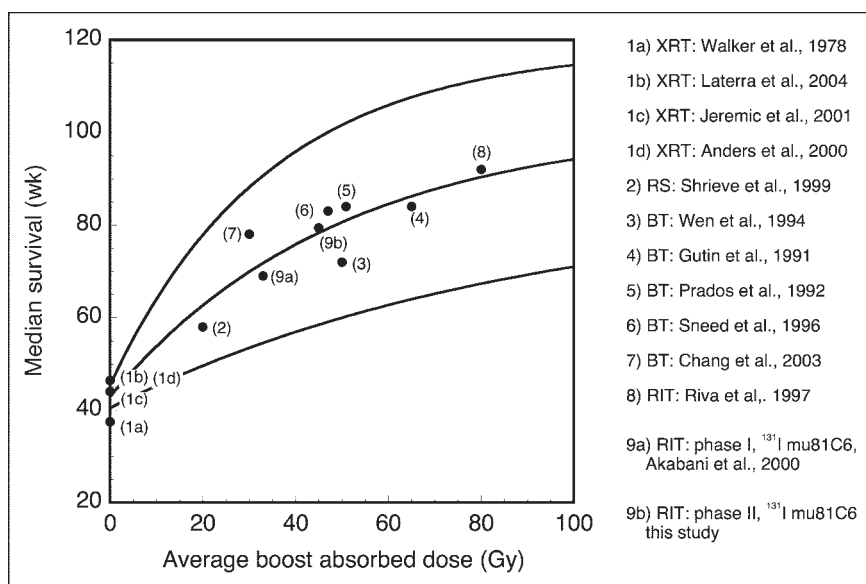


**FIGURE 5.** Regression analysis (95% CI) between average boost absorbed dose and median survival for newly diagnosed GBM patients receiving XRT and radiosurgery, brachytherapy, or RIT. Among the different clinical studies, including ours, an asymptotic increase in median survival as a function of average boost absorbed dose after XRT was observed. Dose estimates for Riva et al. (35) were based on an average residence time of 82 h, average cavity size of  $19 \text{ cm}^3$ , and 5 courses of  $^{131}\text{I}$ -BC2 and BC4 mAbs for a total administered activity of 9,250 MBq. This relationship among studies confirms the relevance of limiting the absorbed dose to tumor foci to minimize normal brain tissue injury and maximize tumor control. Reoperation rates were between 40% and 60% among brachytherapy studies, whereas rate for RIT using  $^{131}\text{I}$ -mu81C6 mAb was 3%. RS = radiosurgery; BT = brachytherapy.

reoperation rates and late adverse events. Conversely, the major advantage of RIT is the potential for the radiolabeled mAb to bind and irradiate preferentially microscopic tumor foci surrounding the cavity while sparing normal brain tissue more efficiently. Nonetheless, we observed that our phase I and phase II studies followed the same trend as brachytherapy. However, for those patients with reversible neurotoxicity, we estimated a median survival of 98 wk; consequently, careful control of the radiation dosage to avoid the onset of irreversible neurotoxicity may be the key factor in maximizing survival using this therapeutic approach. Dosimetric analysis of initial biopsy samples resulted in an optimal absorbed dose of 44 Gy, which maximizes the tumor control while minimizing the induction of radionecrosis by limiting the total absorbed dose to the 2-cm cavity margins to <110 Gy after XRT is administered.

The increased accumulation of mu81C6 mAb around regions of vasogenic edema was observed on registered MRI/SPECT images. The presence of vasogenic edema is consistent with the fact that high-grade malignant gliomas have the ability to disrupt the tight junctions of endothelial cells by secreting soluble factors, such as cell-adhesion molecules and matrix-degrading proteases, leading eventually to changes in the ECM composition and consequent BBB disruption (36). The production of certain ECM molecules—for example, hyaluronic acid, galectins, chondroitin sulfate, TN-C, and the aquaporin-4 (AQP4) protein—is increased in high-grade gliomas and they positively correlate with the migration of glioma cells and production of brain vasogenic edema (37). The overexpression of these ECM molecules correlates with increased tumor malignancy and migratory activity, where these molecules may produce a preferential pathway for tumor cell migration (38,39). Thus, the production of vasogenic edema leads to the formation of a barrier for blood-borne chemotherapeutics that constrains their diffusion process into the brain parenchyma.

In physical terms, these ECM-modifying factors have been shown to increase the physical parameters  $\alpha$  (extracellular space volume fraction),  $\lambda$  (tortuosity), and  $\kappa'$  (non-specific uptake,  $s^{-1}$ ), which govern the trafficking and diffusion of compounds (24,25). Such physical changes lead to an increase in the apparent diffusion coefficient, which is observed in diffusion-weighted images (40,41), and could explain the observed preferential distribution of mu81C6 mAb through regions of vasogenic edema at the time of administration. However, the lack of data regarding the microscopic distribution of  $^{131}\text{I}$ -mu81C6 mAb within the brain parenchyma did not permit us to determine the heterogeneities in its distribution and corresponding doses among the different brain tissue structures (tumor foci and normal tissue structures and vascularity). We anticipate a higher absorbed dose delivered to these tumor foci where TN-C is restricted to the perivascular regions around immature blood vessels and within the fibrillar areas with a netlike diffusive pattern (10,16).

## CONCLUSION

Our results highlight the palliative character of actual radiation therapy, including RIT, in the treatment of high-grade malignant gliomas. However, as established by our phase I and phase II studies,  $^{131}\text{I}$ -mu81C6 mAb is significantly associated with an increase in the median survival in patients with high-grade gliomas with minimal reoperation rates. We also observed the preferential distribution of the radiolabeled mAb through areas of vasogenic edema at the time of therapy, irrespective of cavity size, and observed that irreversible neurotoxicity, regardless of its etiology, is a key predictor of survival. We estimated an optimal target dose of 44 Gy to the 2-cm cavity margins, and further clinical studies are warranted to prove the effectiveness of achieving this target dose rather than administering a fixed activity. Further questions that remain to be addressed for this therapy strategy include the effect vasogenic edema before  $^{131}\text{I}$ -mu81C6 mAb therapy, dose fractionation and escalation, induction of vasogenic edema, tumor control and progression, onset of tissue radionecrosis, and overall median survival.

## ACKNOWLEDGMENTS

This work was supported by the National Center for Research Resources General Clinical Research Centers Program, National Institutes of Health (grants MO1-RR 30, NS20023, CA11898, CA70164, CA42324, 1P50CA108786-01), the Department of Energy (grant DE-FG02-05ER63963), and the American Cancer Society (grant PDT-414).

## REFERENCES

1. Walker MD, Alexander E Jr, Hunt WE, et al. Evaluation of BCNU and/or radiotherapy in the treatment of anaplastic gliomas: a cooperative clinical trial. *J Neurosurg.* 1978;49:333–343.
2. Sheline GE. Radiotherapy for high grade gliomas. *Int J Radiat Oncol Biol Phys.* 1990;18:793–803.
3. Latterra JJ, Grossman SA, Carson KA, et al. Suramin and radiotherapy in newly diagnosed glioblastoma: phase 2 NABTT CNS Consortium Study. *Neurooncol.* 2004;6:15–20.
4. Jeremic B, Shibamoto Y, Grujicic D, et al. Concurrent accelerated hyperfractionated radiation therapy and carboplatin/etoposide in patients with malignant glioma: long-term results of a phase II study. *J Neurooncol.* 2001;51:133–141.
5. Anders K, Grabenbauer GG, Schuchardt U, et al. Accelerated radiotherapy with concomitant ACNU/Ara-C for the treatment of malignant glioma. *J Neurooncol.* 2000;48:63–73.
6. Shrieve DC, Alexander E 3rd, Black PM, et al. Treatment of patients with primary glioblastoma multiforme with standard postoperative radiotherapy and radiosurgical boost: prognostic factors and long-term outcome. *J Neurosurg.* 1999;90:72–77.
7. Chang CN, Chen WC, Wei KC, et al. High-dose-rate stereotactic brachytherapy for patients with newly diagnosed glioblastoma multiformes. *J Neurooncol.* 2003;61:45–55.
8. Cho KH, Hall WA, Lo SS, et al. Stereotactic radiosurgery versus fractionated stereotactic radiotherapy boost for patients with glioblastoma multiforme. *Technol Cancer Res Treat.* 2004;3:41–49.
9. Wen PY, Alexander E 3rd, Black PM, et al. Long term results of stereotactic brachytherapy used in the initial treatment of patients with glioblastomas. *Cancer.* 1994;73:3029–3036.
10. Cai M, Onoda K, Takao M, et al. Degradation of tenascin-C and activity of matrix metalloproteinase-2 are associated with tumor recurrence in early stage non-small cell lung cancer. *Clin Cancer Res.* 2002;8:1152–1156.
11. Zagzag D, Shiff B, Jallo GI, et al. Tenascin-C promotes microvascular cell migration and phosphorylation of focal adhesion kinase. *Cancer Res.* 2002;62:2660–2668.

12. Bigner DD, Brown MT, Friedman AH, et al. Iodine-131-labeled antitenascin monoclonal antibody 81C6 treatment of patients with recurrent malignant gliomas: phase I trial results. *J Clin Oncol*. 1998;16:2202–2212.
13. Akabani G, Reist CJ, Cokgor I, et al. Dosimetry of <sup>131</sup>I-labeled 81C6 monoclonal antibody administered into surgically created resection cavities in patients with malignant brain tumors. *J Nucl Med*. 1999;40:631–638.
14. Akabani G, Cokgor I, Coleman RE, et al. Dosimetry and dose-response relationships in newly diagnosed patients with malignant gliomas treated with iodine-131-labeled anti-tenascin monoclonal antibody 81C6 therapy. *Int J Radiat Oncol Biol Phys*. 2000;46:947–958.
15. Reardon DA, Akabani G, Coleman RE, et al. Phase II trial of murine <sup>131</sup>I-labeled antitenascin monoclonal antibody 81C6 administered into surgically created resection cavities of patients with newly diagnosed malignant gliomas. *J Clin Oncol*. 2002;20:1389–1397.
16. Zagzag D, Capo V. Angiogenesis in the central nervous system: a role for vascular endothelial growth factor/vascular permeability factor and tenascin-C—Common molecular effectors in cerebral neoplastic and non-neoplastic “angiogenic diseases.” *Histol Histopathol*. 2002;17:301–321.
17. McLendon RE, Wikstrand CJ, Matthews MR, et al. Glioma-associated antigen expression in oligodendroglial neoplasms: tenascin and epidermal growth factor receptor. *J Histochem Cytochem*. 2000;48:1103–1110.
18. Zagzag D, Friedlander DR, Dosik J, et al. Tenascin-C expression by angiogenic vessels in human astrocytomas and by human brain endothelial cells in vitro. *Cancer Res*. 1996;56:182–189.
19. Deryugina EI, Bourdon MA. Tenascin mediates human glioma cell migration and modulates cell migration on fibronectin. *J Cell Sci*. 1996;109:643–652.
20. Trotti A, Byhardt R, Stetz J, et al. Common toxicity criteria: version 2.0—An improved reference for grading the acute effects of cancer treatment: impact on radiotherapy. *Int J Radiat Oncol Biol Phys*. 2000;47:13–47.
21. Trotter DEG, Bowsher JE, Stone CD, et al. High-resolution in vivo SPECT imaging of I-131 biodistributions using a rotating parallel-hole collimator. *J Nucl Med*. 1999;40:34–35.
22. Hudson HM, Larkin RS. Accelerated image-reconstruction using ordered subsets of projection data. *IEEE Trans Med Imaging*. 1994;13:601–609.
23. Akabani G, Hawkins WG, Eckblade MB, et al. Patient-specific dosimetry using quantitative SPECT imaging and three-dimensional discrete Fourier transform convolution. *J Nucl Med*. 1997;38:308–314.
24. Schneider SW, Ludwig T, Tatenhorst L, et al. Glioblastoma cells release factors that disrupt blood-brain barrier features. *Acta Neuropathol (Berl)*. 2004;107:272–276.
25. Vargova L, Homola A, Zamecnik J, et al. Diffusion parameters of the extracellular space in human gliomas. *Glia*. 2003;42:77–88.
26. Mishima N, Tamiya T, Matsumoto K, et al. Radiation damage to the normal monkey brain: experimental study induced by interstitial irradiation. *Acta Med Okayama*. 2003;57:123–131.
27. Marriott CJ, Thorstad W, Akabani G, et al. Locally increased uptake of fluorine-18-fluorodeoxyglucose after intracavitary administration of iodine-131-labeled antibody for primary brain tumors. *J Nucl Med*. 1998;39:1376–1380.
28. Leibel SA, Gutin PH, Davis RL. Factors affecting radiation injury after interstitial brachytherapy for brain tumors. In: Gutin PH, Leibel SA, Sheline GE, eds. *Radiation Injury to the Nervous System*. New York, NY: Raven Press; 1991: 257–270.
29. Hoshino T. Cell kinetics of glial tumors. *Rev Neurol (Paris)*. 1992;148:396–401.
30. Walker AE, Robins M, Weinfeld FD. Epidemiology of brain tumors: the National Survey of Intracranial Neoplasms. *Neurology*. 1985;35:219–226.
31. Gutin PH, Prados MD, Phillips TL, et al. External irradiation followed by an interstitial high activity iodine-125 implant “boost” in the initial treatment of malignant gliomas: NCOG Study 6G-82-2. *Int J Radiat Oncol Biol Phys*. 1991; 21:601–606.
32. Prados MD, Schold SJS, Fine HA, et al. A randomized, double-blind, placebo-controlled, phase 2 study of RMP-7 in combination with carboplatin administered intravenously for the treatment of recurrent malignant glioma. *Neurooncol*. 2003;5:96–103.
33. Sneed PK, Russo C, Scharfen CO, et al. Long-term follow-up after high-activity <sup>125</sup>I brachytherapy for pediatric brain tumors. *Pediatr Neurosurg*. 1996;24:314–322.
34. Prados MD, Gutin PH, Phillips TL, et al. Interstitial brachytherapy for newly diagnosed patients with malignant gliomas: the UCSF experience. *Int J Radiat Oncol Biol Phys*. 1992;24:593–597.
35. Riva P, Franceschi G, Arista A, et al. Local application of radiolabeled monoclonal antibodies in the treatment of high grade malignant gliomas: a six-year clinical experience. *Cancer*. 1997;80:2733–2742.
36. Chintala SK, Tonn JC, Rao JS. Matrix metalloproteinases and their biological function in human gliomas. *Int J Dev Neurosci*. 1999;17:495–502.
37. Warth A, Kroger S, Wolburg H. Redistribution of aquaporin-4 in human glioblastoma correlates with loss of agrin immunoreactivity from brain capillary basal laminae. *Acta Neuropathol (Berl)*. 2004;107:311–318.
38. Hayen W, Goebeler M, Kumar S, et al. Hyaluronan stimulates tumor cell migration by modulating the fibrin fiber architecture. *J Cell Sci*. 1999;112:2241–2251.
39. Camby I, Belot N, Rorive S, et al. Galectins are differentially expressed in supratentorial pilocytic astrocytomas, astrocytomas, anaplastic astrocytomas and glioblastomas, and significantly modulate tumor astrocyte migration. *Brain Pathol*. 2001;11:12–26.
40. Castillo M, Smith JK, Kwock L, et al. Apparent diffusion coefficients in the evaluation of high-grade cerebral gliomas. *AJNR*. 2001;22:60–64.
41. Provenzale JM, McGraw P, Mhatre P, et al. Peritumoral brain regions in gliomas and meningiomas: investigation with isotropic diffusion-weighted MR imaging and diffusion-tensor MR imaging. *Radiology*. 2004;232:451–460.